Enhancing spin state phase separation by strontium addition in the Y $(Ba_{1-x}Sr_x)Co_2O_{5.5}$ layered cobaltite

2009 J. Phys.: Condens. Matter 21 326002

(http://iopscience.iop.org/0953-8984/21/32/326002)

J. Phys.: Condens. Matter **21** (2009) 326002 (6pp) doi:10.1088/0953-8984/21/32/326002

Enhancing spin state phase separation by strontium addition in the $Y(Ba_{1-x}Sr_x)Co_2O_{5.5}$ layered cobaltite

G Aurelio[1], J Curiale[1,2], R D Sánchez[1,2] and G J Cuello[3,4]

[1] Consejo Nacional de Investigaciones Científicas y Técnicas, Centro Atómico Bariloche—Comisión Nacional de Energía Atómica, Avenida Bustillo 9500, 8400 San Carlos de Bariloche, RN, Argentina
[2] Instituto Balseiro, Universidad Nacional de Cuyo, Avenida Bustillo 9500, 8400 San Carlos de Bariloche, RN, Argentina
[3] Department of Applied Physics II, Ikerbasque, UPV/EHU, E-48080 Bilbao, Spain
[4] Institut Laue Langevin, F-38042 Grenoble, France

E-mail: gaurelio@cab.cnea.gov.ar

Received 7 May 2009, in final form 27 June 2009
Published 14 July 2009
Online at stacks.iop.org/JPhysCM/21/326002

Abstract

In this paper we present a neutron diffraction study of the effects of replacing Ba with smaller Sr cations in the layered cobaltite $YBaCo_2O_{5+\delta}$ for $\delta \approx 0.5$. Neutron thermodiffractograms are reported in the temperature range 20 K $\leqslant T \leqslant$ 300 K, as well as high-resolution neutron diffraction experiments at selected temperatures. The systematic refinement of the series of samples with Sr substituting at the Ba site permits the understanding of the complex magnetic behaviour of this system, and reinforces a two-phase scenario for the parent compound. We have found that Sr addition destabilizes the ferrimagnetic spin state ordered phase, as well as the '122' order characteristic of cobaltites with $\delta = 0.5$, favouring instead a tetragonal and less ordered structure.

(Some figures in this article are in colour only in the electronic version)

1. Introduction

Cobalt-based magnetic oxides present an extremely rich variety of phenomena. Among them, the layered compounds $RBaCo_2O_{5+\delta}$ (R being a rare earth) are currently being intensively studied [1–12]. They allow for a wide range of oxygen non-stoichiometry which controls the mixed valence state of Co ions, and their physical properties may be tuned by the interplay of several factors: the R cation size, the vacancy structural order, and—as we have shown recently [7]—the disorder introduced by doping the Ba site with smaller cations.

Of particular interest is the case $\delta = 0.5$, for which Co is expected to be completely in the +3 valence state. In this case, a particular order of oxygen vacancies leads to the so-called '122' superstructure, consisting of an ordered array of 50% Co atoms in octahedral oxygen coordination and 50% in a pyramidal environment. The structure is related to a basic perovskite by doubling the cell along the b axis due to the pyramid/octahedron ordering and along the c axis due to the stacking sequence of $[CoO_2]$–[BaO]–$[CoO_2]$–$[RO_\delta]$ planes.

There still remain some controversies regarding the spin states of Co ions and their transitions. The Co^{3+} ion can adopt three possible spin states (low spin, intermediate spin and high spin) as a function of crystallographic environment and temperature. Moreover, there is strong evidence indicating that these compounds adopt spin state ordered (SSO) states in which the spin state not only is different between Co atoms located at pyramids and octahedra, but is also different among the pyramidal [3] or the octahedral sites [4, 7, 9, 13] in ordered arrays. Two SSO phases have been reported at different temperature ranges, corresponding to ferrimagnetic [4, 7, 13] and antiferromagnetic (AFM) configurations [4, 7, 9]. The particular low temperature AFM arrangements are still, however, a subject of controversies. Some authors claim that there is no evidence of the additional doubling of the a-axis associated with the SSO, and adopt instead canted AFM models to explain the neutron diffraction data [14, 5, 10]. But even when there may be no evidence of a '222' superstructure in cobaltites with R = Gd and Pr [5] the case might be different for other lanthanides. In fact, some studies using

NMR techniques showed that for R = Y there are four non-equivalent Co sites at low temperature [15], and for R = Eu there are three [16], which support the SSO models. More recently, we have proposed for the compound with R = Y a two-phase scenario, which consists of a ferrimagnetic SSO phase transforming to an AFM phase at 250 K, accompanied by a second phase showing no ferrimagnetic order but a paramagnetic to AFM transition at ∼200 K [7]. This means that at $T < 200$ K the system presents the coexistence of two different AFM arrangements. We arrived at this picture after a systematic study of the replacement of Ba by Ca, which strongly stabilizes the SSO ferrimagnetic phase in detriment of the AFM order. Shortly after, another diffraction study of the undoped Y compound by Khalyavin *et al* [9], combined with a detailed symmetry analysis, confirmed the low temperature phase coexistence of two orthorhombic phases with AFM order. Luetkens *et al* [8] offered further support to this picture: using muon-spin relaxation measurements, they identified coexisting phases with different spin state arrangements and proposed, also, a phase separation scenario.

In this work we present new neutron diffraction measurements of a second series of doped samples in which the Ba ion has been replaced with 5 and 10% Sr, synthesized under identical conditions to the Ca-doped samples [7]. We had already found strong effects on the magnetic properties when doping the Ba site with Ca, and now we explore the effect of a second dopant, Sr. We will show that the ferrimagnetic phase results quickly destabilized in favour of the combination of two AFM states, even when the incorporation of Sr reduces lattice distortions, favouring a tetragonal symmetry.

2. Experimental methods

Polycrystalline samples of the compound $Y(Ba_{1-x}Sr_x)Co_2O_{5.5}$ with $x_{Sr} = 0.05$ and 0.10 were prepared by solid-state reaction. A single batch was used for these samples and the Ca-substituted samples described in [7], to guarantee identical synthesis conditions, which resulted in samples of about 1.5 g and an oxygen content of $\delta = 0.48 \pm 0.02$ determined by refinement of neutron diffraction (ND) data.

Neutron thermodiffraction data were collected on the high-intensity two-axis diffractometer D20 located at the High Flux Reactor of Institute Laue Langevin (ILL), Grenoble, France, using a wavelength of 2.419 Å. In addition, high-resolution ND data were collected at diffractometer Super-D2B of ILL for the sample with $x_{Sr} = 0.10$. A wavelength of ∼1.594 Å was used to collect patterns at 70, 230 and 348 K for approximately 3 h. Details are described in [7]. The ND patterns were processed with the full-pattern analysis Rietveld method, using the program FULLPROF [17] for refining the crystal and magnetic structures. The strategy for the refinement has been described in [7].

3. Results

The first structural description reported for the parent compound $YBaCo_2O_{5+\delta}$ [18] showed different possible room temperature structures. In particular, for $\delta = 0.5$, we can find an orthorhombic $Pmmm$ phase having the superstructure $a_P \times 2a_P \times 2a_P$ (where a_P denotes the pseudocubic lattice parameter of the related perovskite unit cell), and a so-called '112' phase with no ordering between pyramids and octahedra, having either orthorhombic ($Pmmm$ space group) or tetragonal ($P4/mmm$ space group) symmetry in a $a_P \times a_P \times 2a_P$ cell [18]. After intensive research, it is now accepted that the correct orthorhombic space group allowing for the magnetic arrangements is in fact $Pmma$ with a $2a_P \times 2a_P \times 2a_P$ lattice and four non-equivalent sites for Co atoms. Furthermore, a second orthorhombic phase must be considered even at room temperature to correctly describe diffraction data [7, 19]. On the other hand, the existence of a less distorted tetragonal phase in this system ($P4/mmm$) is usually associated with δ values below 0.5, for which there is no structural order of pyramids and octahedra. However, it seems that the replacement of Sr at the Ba site also favours a $a_P \times a_P \times 2a_P$ tetragonal phase even for $\delta = 0.5$.

Our high-resolution ND data for the sample $x_{Sr} = 0.10$ show, for all temperatures, again the coexistence of two nuclear phases: a prevailing tetragonal (T) phase in the $P4/mmm$ space group with an $a_P \times a_P \times 2a_P$ cell, and a smaller amount of the orthorhombic $Pmma$ phase (O) with an $2a_P \times 2a_P \times 2a_P$ cell. The same two phases are also present in the sample $x_{Sr} = 0.05$, although in this case phase fractions are inverted. To highlight this we show in figure 1 diffraction data from D20 in the interplanar distance (d) range showing some relevant Bragg reflections: $(4\ 0\ 0)_O$, $(0\ 4\ 0)_O$ for the O-phase and $(2\ 0\ 0)_T$ for the T-phase, indicated by vertical bars at the bottom of panel (c). Data collected at different temperatures for sample $x_{Sr} = 0.05$ are shown in (a), while panel (b) corresponds to sample $x_{Sr} = 0.10$. The presence of the O-phase is revealed by the distortion occurring above 295 K, in which the lattice parameters a and b suddenly change at the metal–insulator transition [7]. This results in a shift of the $(4\ 0\ 0)_O$ and $(0\ 4\ 0)_O$ reflections, clearly observed in figure 1(a). The T-phase, on the other hand, does not undergo any sharp cell distortion which makes it easier to distinguish the two phases above room temperature by inspection of these reflections. In both cases, there is a majority phase (O in $x_{Sr} = 0.05$, T in $x_{Sr} = 0.10$) and a smaller amount of the other one. Figure 1(c) shows the data collected at D2B for the same reflections, where the presence of O-phase is better resolved at 348 K (arrows point to the shoulders that reveal the orthorhombic distortion).

Structural details for the T-phase are given in table 1, obtained from the refinement of D2B data for sample $x_{Sr} = 0.10$ at 70, 230 and 348 K. The occupation of oxygen was refined for the 1b Wyckoff position, corresponding to the O2 oxygen atom lying in the $[Y\ O]_\delta$ plane, and it indicates no significant deviation from the nominal $\delta = 0.5$ value. For the coexisting O-phase, the refinement was conducted with the atomic coordinates and atomic thermal parameters fixed at the values reported in [9] to avoid excessive free parameters in the minority phase. The oxygen occupation in the $[Y\ O]_\delta$ layer of the O-phase (site O7 in the notation of [9]) was allowed to vary in the refinement, to explore a possible oxygen segregation among the two coexisting phases. This was not observed—within the limitations of the experimental conditions—and the

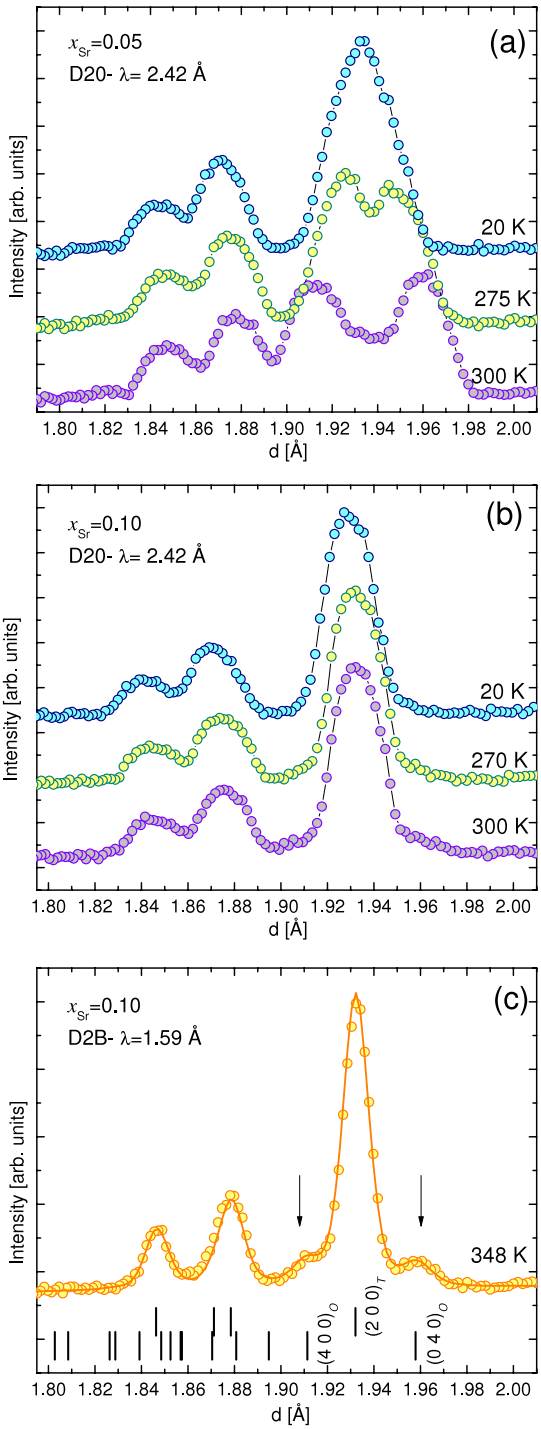

Figure 1. Neutron diffractograms collected at D20 and D2B for the interplanar distance range 1.80 Å $< d <$ 2.00 Å showing the Bragg reflections $(4\,0\,0)_O$, $(0\,4\,0)_O$ and $(2\,0\,0)_T$ for the O and T phases. (a) Data for sample $x_{Sr} = 0.05$ collected at D20. (b) Data for sample $x_{Sr} = 0.10$ collected at D20. (c) Data collected at D2B for sample $x_{Sr} = 0.10$. The line corresponds to the Rietveld refinement. The arrows indicate the presence of the distorted O-phase at 348 K. The vertical bars at the bottom represent Bragg reflections from the O- and T-phases. For clarity, only the most relevant are labelled.

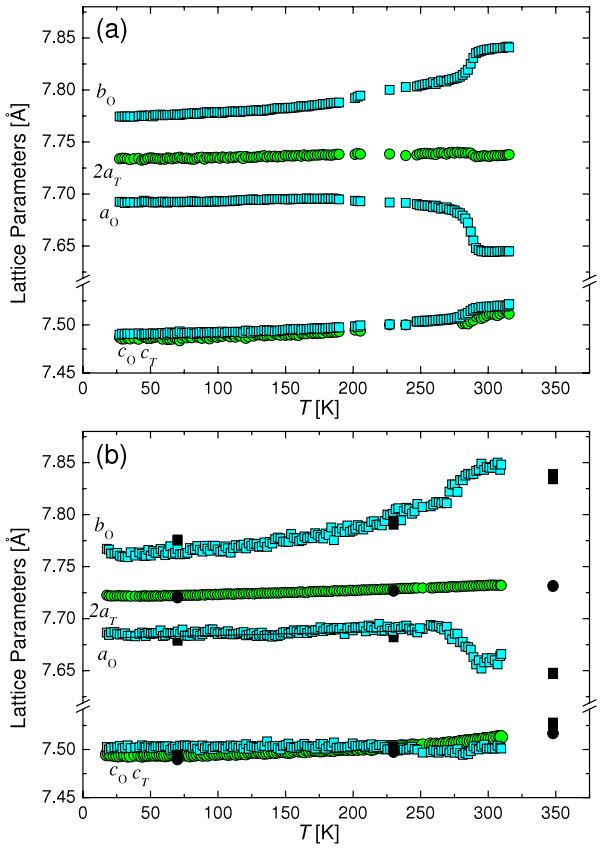

Figure 2. Thermal evolution of the lattice parameters a_O, b_O and c_O for the O-phase (square symbols) and $2a_T$ and c_T for the T-phase (circles) in samples with $x_{Sr} = 0.05$ (a) and $x_{Sr} = 0.10$ (b), determined from data collected at D20 and D2B (solid symbols in (b)).

oxygen content of the O-phase agrees with the global oxygen content of the samples. Anyway, the O-phase is not expected to deviate significantly from the value $\delta = 0.5$, as will become clearer in the following discussion. For the sample $x_{Sr} = 0.05$ we do not present structural data, as this sample was not measured at the D2B instrument. Thermodiffraction data for this sample were refined with fixed atomic coordinates coming from the $x_{Sr} = 0.10$ sample refinement shown in table 1 for the T-phase, and data from [9] for the O-phase.

The evolution with temperature of the lattice parameters refined in the O- and T-phases is shown in figure 2 for both samples. In figure 2(b) the sequential D20 results are presented together with the results from D2B at the studied temperatures. For the O-phase, the distortion just above room temperature is clearly confirmed, as we had already observed in the samples with $x_{Ca} = 0, 0.05$ and 0.10. This is another reason to expect the O-phase to have an oxygen content very close to the nominal value $\delta = 0.5$.

With the nuclear phases clarified, we now turn to the magnetic diffraction observed in our samples, summarized in figure 3. The thermodiffractogram for sample $x_{Sr} = 0.05$ reveals a complex behaviour with temperature. In the top panels of figure 3 we present three different sections of the projected thermodiffractogram for the sample $x_{Sr} = 0.05$, in which most reflections are of magnetic nature. We have refined these data by assuming a model in which the O-phase behaves the same way as in the parent compound $YBaCo_2O_{5.5}$, i.e., it becomes ferrimagnetic and presents SSO below 282 K [7, 4].

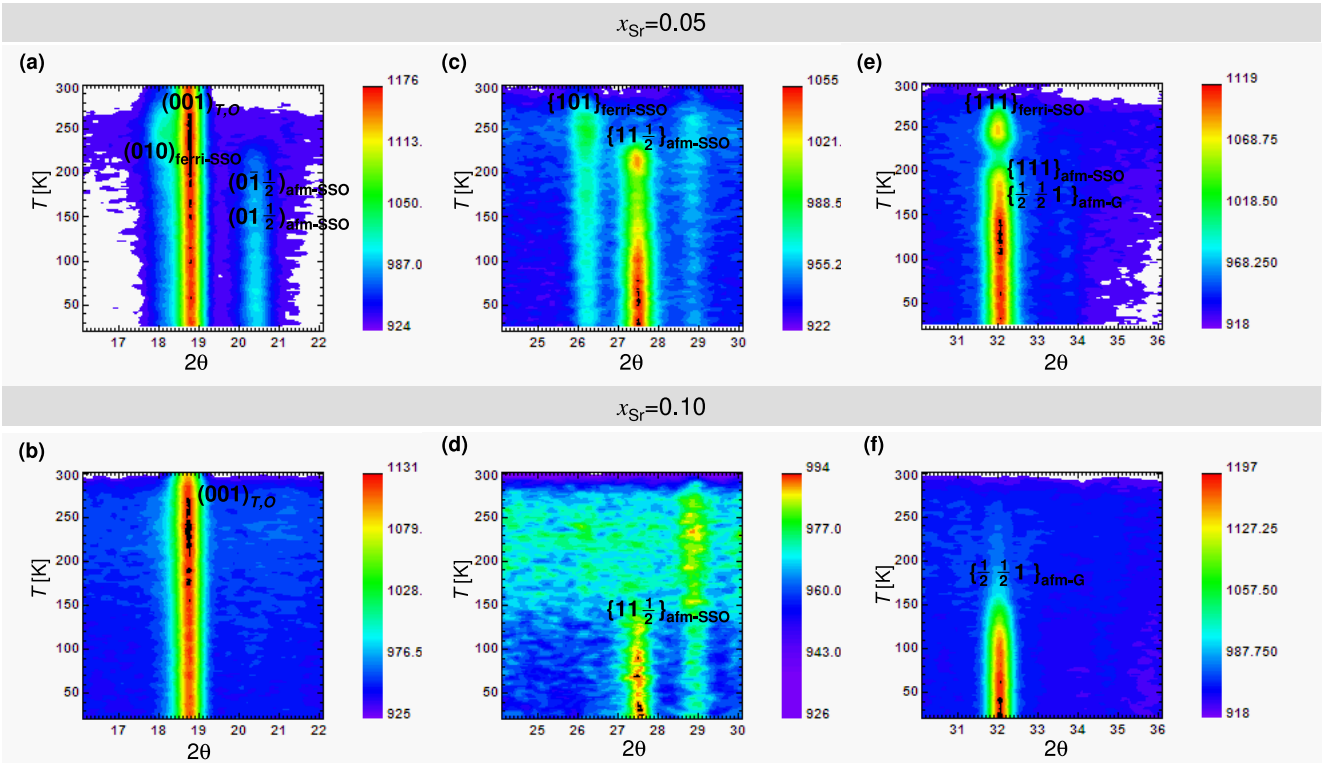

Figure 3. Projection of three selected sections of the thermodiffractograms corresponding to samples with $x_{Sr} = 0.05$ (upper panels) and $x_{Sr} = 0.10$ (bottom panels). (a), (b) $16° < 2\theta < 22°$, (c), (d) $24° < 2\theta < 30°$ and (e), (f) $30° < 2\theta < 36°$, showing the major magnetic reflections. Reflections were indexed based on the nuclear cells of the O- and T-phases. Data were collected at D20 with $\lambda \sim 2.42$ Å in the temperature range 20–310 K, and plotted using the LAMP software [23].

Table 1. Structural parameters refined from the high-resolution D2B data for the T-phase in the compound $YBa_{0.90}Sr_{0.10}Co_2O_{5.5}$ at $T = 70$, 230 and 348 K. Atomic fractional coordinates for the T-phase correspond to space group $P4/mmm$ in the following Wyckoff positions: Y (1d) = $(\frac{1}{2}, \frac{1}{2}, \frac{1}{2})$; Ba, Sr (1c) = $(\frac{1}{2}, \frac{1}{2}, 0)$; Co (2g) = $(0, 0, z)$; O1 (1a) = $(0, 0, 0)$; O2 (1b) = $(0, 0, \frac{1}{2})$; O3 (4i) = $(0, \frac{1}{2}, z)$. The coexisting O-phase refined lattice parameters are also indicated.

$P4/mmm$		$T = 70$ K	$T = 230$ K	$T = 348$ K
Co	z	0.2523(1)	0.2528(7)	0.2540(7)
O3	z	0.2952(3)	0.2953(1)	0.2953(2)
O2	Occ.	0.49(1)	0.48(1)	0.48(1)
a_T (Å)		3.8600(6)	3.8632(4)	3.8655(3)
c_T (Å)		7.4894(2)	7.4972(2)	7.516(1)
a_O (Å)		7.678(1)	7.682(1)	7.648(1)
b_O (Å)		7.776(1)	7.794(1)	7.834(1)
c_O (Å)		7.494(1)	7.502(1)	7.526(1)
R_{B_T}		7.0	7.6	7.0
χ^2		7.0	5.3	5.4

For this ferrimagnetic phase, with a magnetic cell $2a_P \times 2a_P \times 2a_P$, the reflections (labelled 'ferri-SSO' in figure 3) increase in intensity between 282 and 240 K and then decrease to smaller values on cooling. This feature mimics the thermal evolution of the macroscopic low-field magnetization of the sample, shown in figure 4(a) with circles (right axis), as well as that of the parent compound. The reason for the decrease in the global magnetization is the transition of the O-phase from the ferrimagnetic SSO state to an SSO-AFM state. Actually, we can see in figures 3(a) and (c) that the decrease of the intensity of the 'ferri-SSO' reflections is concomitant with the occurrence of new reflections corresponding to a magnetic $2a_P \times 2a_P \times 4a_P$ cell, which are labelled 'afm-SSO'. The best magnetic model for this phase proved to be that in which there is still a SSO between adjacent octahedron chains along the a-axis, but a global AFM arrangement of spins, as described in [9]. A very similar model is found in [8] based on a completely different technique, namely, muon-spin relaxation. This magnetic configuration, in our sample as well as in the parent compound, stays the same down to the lowest temperature studied.

The thermodiffractogram also shows that between 215 and 185 K there is a small decrease in the O-phase fraction, which makes the $\{11\frac{1}{2}\}_{afm-SSO}$ set of reflections at $2\theta = 27.5$ decrease in intensity (figure 3(c)). Below 185 K, they grow again due to the increase of the magnetic moment of Co with decreasing temperature and to the onset of yet another set of magnetic reflections: the T-phase adopts an AFM order with a magnetic $2a_P \times 2a_P \times 2a_P$ cell (labelled 'afm-G' in figure 3). As there is no particular structural order between octahedra and pyramids in the T-phase, the simplest AFM model is of G type, i.e., every Co atom—at any site—surrounded by neighbours having an opposite spin direction, as is observed in $HoBaCo_2O_{5+\delta}$ [20]. Our data do not allow us to distinguish whether there is a structural $P4/mmm$ to $Pmmm$ transition at the onset of the G-type AFM behaviour, as observed in

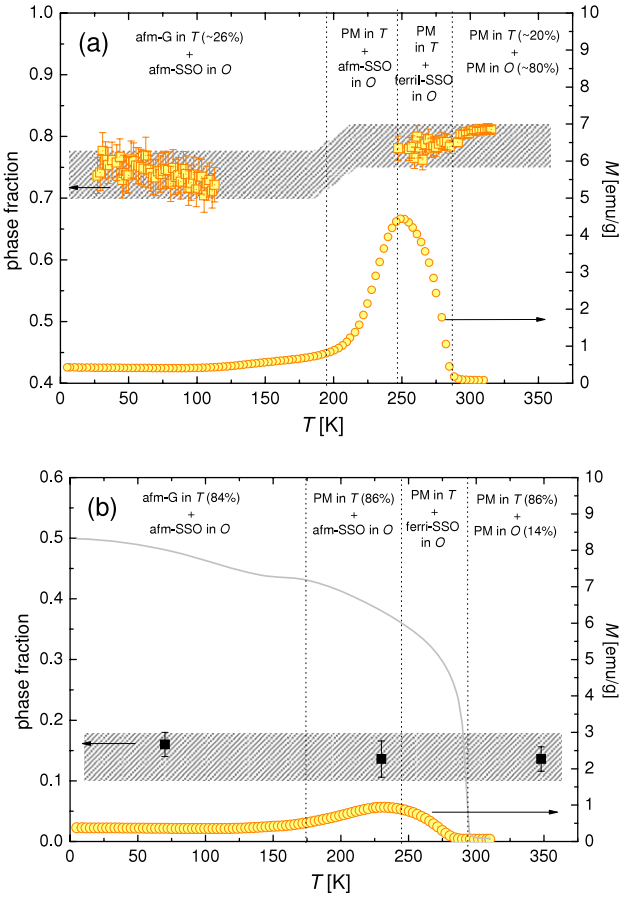

Figure 4. Thermal evolution of the O-phase fraction (left axes, squares) determined from D20 data and macroscopic low-field magnetization (right axes, circles) in samples with $x_{Sr} = 0.05$ (a) and $x_{Sr} = 0.10$ (b). Solid squares correspond to values refined from high-resolution D2B data. The hatched areas correspond to the estimated evolution of phase fractions. The grey curve in (b) corresponds to the magnetization of the sample with $x_{Ca} = 0.10$, shown as a reference sample with 100% O-phase [7]. In all cases, the low-field magnetization was measured on cooling under a magnetic field of 5 kOe.

$YBaCo_2O_5$ [21, 22], so the refinements below 185 K for the nuclear T-phase were also performed in the $P4/mmm$ space group. The presence of AFM order in the T-phase may not be evident just from inspection in the thermodiffractogram of sample $x_{Sr} = 0.05$, but it is a necessary ingredient of the overall model, and will become clearer for sample $x_{Sr} = 0.10$. Below 185 K, there is therefore a magnetic phase coexistence between two AFM arrangements. A scheme of the phase diagram for the $x_{Sr} = 0.05$ sample is presented in figure 4(a). When possible, phase fractions were refined (symbols in figure 4). In other cases, due to the extreme coupling of parameters, we have just sketched as a hatched area the probable behaviour of phase fractions based on all the above information.

For the sample with $x_{Sr} = 0.10$, in which the majority phase is T the whole time, the situation is analogous to that in the $x_{Sr} = 0.05$ sample. The only difference lies in the relative phase fractions, which make the thermodiffractogram (figures 3(b), (d) and (f)) look quite different. The smaller

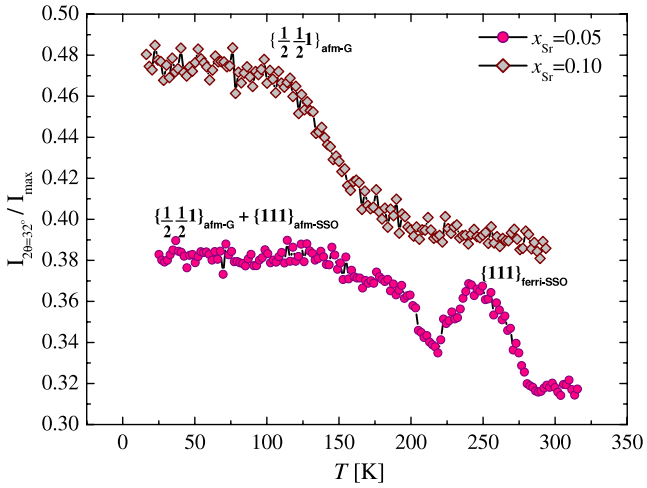

Figure 5. Thermal evolution of the intensity of the reflection at $2\theta \sim 32°$ (figures 3(e) and (f)) relative to the most intense nuclear reflection, corresponding to the contribution of the $(1\ 1\ 2)_T$ and $(2\ 2\ 2)_O$ Bragg reflections, from D20 data in samples with $x_{Sr} = 0.05$ and 0.10.

amount of O-phase present at room temperature (14%), confirmed by the high-resolution data from D2B at 348 K, becomes ferrimagnetic ('ferri-SSO') and then AFM ('afm-SSO'); which explains the similar shape of the magnetization curve but its lower values, with respect to the parent compound and to the $x_{Sr} = 0.05$ sample. The T-phase again transforms to a G-type AFM below 180 K with a $2a_P \times 2a_P \times 2a_P$ cell ('afm-G'), whose most intense reflection occurs at $2\theta \sim 32°$ (figure 3(f)). To further understand this picture, we present in figure 5 for samples $x_{Sr} = 0.05$ and 0.10 the evolution with temperature of the intensity of the reflection at $2\theta \sim 32°$ relative to the most intense nuclear reflection, given by the contributions of the $(1\ 1\ 2)_T$ and $(2\ 2\ 2)_O$ Bragg reflections. The indexation at each temperature interval is based on the nuclear cells $2a_P \times 2a_P \times 2a_P$ for the O-phase and $a_P \times a_P \times 2a_P$ for the T-phase. The low temperature behaviour mimics the evolution of the microscopic magnetic moment of Co atoms in the samples averaged between the magnetic phases. The increase in intensity at low temperature with respect to the paramagnetic high temperature state is very similar in both samples. Finally, in figure 4(b) we present the phase fraction of the O-phase, which remains almost constant, as well as the low-field magnetization and a scheme of the phase diagram for the sample $x_{Sr} = 0.10$.

The analysis of the data was not limited to just identifying the magnetic cells, but the most plausible magnetic models that account for the diffraction data were included in the refinements. However, given the multiphasic scenario, several constraints had to be introduced. We do not present here further details of any refinement of the D20 data, as that is not the scope of the present work. To obtain better magnetic and structural details, new experiments should be conducted focusing on each of the phases of interest which we have now consistently identified. Diffraction experiments in such a complex system need more statistics and resolution to grasp the details. Our goal, instead, has been to give a broad

overall insight on the phase diagram and to offer a consistent picture.

4. Concluding remarks

Among the layered cobaltites $RBaCo_2O_{5.5}$ reported in the literature, it seems that the use of a small cation such as yttrium at the R site favours multiphasic samples, with a more complex magnetic behaviour than when using rare earth cations with larger radii. The combined results from our previous and present study, through the use of cation substitution, have allowed us to disentangle the contributions and features which characterize each possible phase in the system. After these studies, as well as some others [15, 16, 8, 9, 19], we are certain that a two-phase scenario is needed to account for the complete set of experimental facts about this system. As we mentioned before, our aim was not to give details about each structural and magnetic phase, but to clarify the global behaviour of these cobaltites. To this end, we have explored a rather large area of the phase space, mapping different variables such as dopants, dopant concentrations, and temperature. We arrive here at a consistent picture which accounts for all our experimental observations. A key contribution of the present work consists in showing how each phase that coexists in the parent compound can actually be stabilized by the local disorder introduced by substituting small amounts of Ba with other cations. This could be a good method to obtain monophasic samples in which to isolate and study other magnetic, electric and electronic properties. Our next step will focus on the short-range environment of Co atoms, to understand why the substitution at the Ba site affects so much the magnetism of the system and the stability of different structural configurations.

Acknowledgments

This work is part of a research project supported by Agencia Nacional de Promoción Científica y Tecnológica (Argentina), under grants PICT 17-21372 and 20144, and by SECTyP, Universidad Nacional de Cuyo. JC acknowledges a fellowship from CNEA and CONICET. We particularly acknowledge ILL and its staff for the beamtime allocation and technical assistance.

References

[1] Taskin A A, Lavrov A N and Ando Y 2005 *Phys. Rev.* B **71** 134414
[2] Frontera C, Caneiro A, Carrillo A E, Oró-Solé J and García-Muñoz J L 2005 *Chem. Mater.* **17** 5439
[3] Plakhty V P, Chernenkov Yu P, Barilo S N, Podlesnyak A, Pomjakushina E, Moskvin E V and Gavrilov S V 2005 *Phys. Rev.* B **71** 214407
[4] Khalyavin D D 2005 *Phys. Rev.* B **72** 134408
[5] Frontera C, García-Muñoz J L, Carrillo A E, Aranda M A G, Margiolaki I and Caneiro A 2006 *Phys. Rev.* B **74** 054406
[6] Khalyavin D D, Argyriou D N, Amann U, Yaremchenko A A and Kharton V V 2007 *Phys. Rev.* B **75** 134407
[7] Aurelio G, Curiale J, Sánchez R D and Cuello G J 2007 *Phys. Rev.* B **76** 214417
[8] Luetkens H, Stingaciu M, Pashkevich Yu G, Conder K, Pomjakushina E, Gusev A A, Lamonova K V, Lemmens P and Klauss H-H 2008 *Phys. Rev. Lett.* **101** 017601
[9] Khalyavin D D, Argyriou D N, Amann U, Yaremchenko A A and Kharton V V 2008 *Phys. Rev.* B **77** 064419
[10] Frontera C, García-Muñoz J L and Castano O 2008 *J. Appl. Phys.* **103** 07F713
[11] Díaz-Fernández Y, Malavasi L and Mozzati M C 2008 *Phys. Rev.* B **78** 144405
[12] Motin Seikh Md, Simon Ch, Caignaert V, Pralong V, Lepetit M B, Boudin S and Raveau B 2008 *Chem. Mater.* **20** 231
[13] Fauth F, Suard E, Caignaert V and Mirebeau I 2002 *Phys. Rev.* B **66** 184421
[14] Soda M, Yasui Y, Fujita T, Miyashita T, Sato M and Kakurai K 2003 *J. Phys. Soc. Japan* **72** 1729
[15] Itoh M, Nawata Y, Kiyama T, Akahoshi D, Fujiwara N and Ueda Y 2003 *Physica* B **329–333** 751
[16] Kubo H, Zenmyo K, Itoh M, Nakayama N, Mizota T and Ueda Y 2004 *J. Magn. Magn. Mater.* **272–276** 581
[17] Rodríguez-Carvajal J 1990 FULLPROF: a program for Rietveld refinement and pattern matching analysis *Abstracts of the Satellite Mtg on Powder Diffraction of the XV Congr. of the IUCr (Toulouse)* p 127
[18] Akahoshi D and Ueda Y 1999 *J. Phys. Soc. Japan* **68** 736
[19] Bobrovskii V, Kazantsev V, Mirmelstein A, Mushnikov N, Proskurnina N, Voronin V, Pomjakushina E, Conder K and Podlesnyak A 2009 *J. Magn. Magn. Mater.* **321** 429
[20] Malavasi L, Diaz-Fernandez Y, Mozzati M C and Ritter C 2008 *Solid State Commun.* **148** 87
[21] Vogt T, Woodward P M, Karen P, Hunter B A, Henning P and Moodenbaugh A R 2000 *Phys. Rev. Lett.* **84** 2969
[22] Fauth F, Suard E, Caignaert V, Domengès B, Mirebeau I and Keller L 2001 *Eur. Phys. J.* B **21** 163
[23] *LAMP, the Large Array Manipulation Program* http://www.ill.fr/data_treat/lamp/front.html